Applications in Energy and Combustion Science 18 (2024) 100260

Contents lists available at ScienceDirect

Applications in Energy and Combustion Science

journal homepage: www.elsevier.com/locate/jaecs

Characterization of a 5-nozzle array using premix/micromix injection for hydrogen

Antoine Durocher [a,b], Luming Fan [a], Marc Füri [c], Gilles Bourque [b,c], Julien Sirois [c], David May [c], Jeffrey M. Bergthorson [b], Sean Yun [a], Patrizio Vena [a,d,*]

[a] Gas Turbine Laboratory (GTL) - Zero Carbon Technology, National Research Council Canada, Ottawa, Ontario, Canada
[b] Alternative Fuels Laboratory (AFL) - Department of Mechanical Engineering, McGill University, Montréal, Québec, Canada
[c] Siemens Energy, Montréal, Québec, Canada
[d] École Polytechnique Montréal, Montréal, Québec, Canada

ARTICLE INFO

Keywords:
Hydrogen flame
Micromix
OH-PLIF
Multi-nozzle array

ABSTRACT

Hydrogen is one of the most promising fuels to decarbonize energy systems since it has a high specific energy, a carbon-free combustion process, and may be produced sustainably through electrolysis. Direct fuel drop-in replacement cannot be done in traditional lean, premixed combustion burners because of the high reactivity of the hydrogen-air mixture and its inherently unstable nature that might lead to flashback and hardware failure. Consequently, new injection strategies and burner geometries are investigated to mitigate these risks. Here we present hydrogen capabilities of a premix/micromix injector that relies on a two-staged fuel injection strategy to offer wide fuel flexible capability (methane to hydrogen) within a single design. Five injectors are placed in a cross-shaped array to simulate a sector found in multi-element combustion systems. Stability and combustion dynamics maps are obtained for the array and OH planar laser-induced fluorescence (PLIF) provides additional insight into the combustion process of these novel burners when placed in an array. The use of micromixing is shown to drastically improve the acoustics of this geometry and expand the flashback limits compared to the fully premixed configuration. Significant variability in flashback limits are observed for different additively-manufactured injector configurations. Phase-averaged OH-PLIF measurements, obtained by registering the acquisition with the acoustics module, and the 3D reconstruction of a partially-premixed flame highlight the complexity of the stabilization mechanisms for these highly three-dimensional, non-axisymmetric flames that may be subjected to large thermoacoustics. This first investigation into premix/micromix clustered injectors demonstrates the importance of better understanding the impact of flame–flame interaction in multi-element combustion systems with micromixed, or partially-premixed, combustion.

1. Introduction

Hydrogen has received significant interest as the leading alternative to carbon-based fuels in an effort to decarbonize the energy sector. While it could potentially offer a high specific energy, the combustion of hydrogen in gas turbine engines still faces many challenges. Notwithstanding the production, delivery, and storage of such large quantities of hydrogen [1,2], the technology needed to safely and sustainably burn hydrogen has yet to be identified. The established dry-low-NO_x technology that was developed to minimize nitric oxide emissions (NO_x) from hydrocarbon fuels cannot be used directly for hydrogen-fueled gas turbines, where three challenges are generally raised for the use of high-hydrogen content fuels in these lean, and ultra-lean, premixed systems: hardware damage resulting from the increased risk of flashback, hardware damage resulting from thermoacoustic instabilities, and emissions control since potentially higher flame temperatures could lead to increased NO_x formation [3–6].

Different combustion strategies have been investigated to allow industrial gas turbine systems to run with high hydrogen content. While details on the implementation, designs, and operating conditions might vary from one proposed strategy to another, many hydrogen fueling strategies appear to rely on fuel staging, partially-premixed conditions, and/or the miniaturization of flames. Sequential combustors have been demonstrated by Ansaldo Energia to be able to burn high hydrogen content fuels by using predominantly autoignition as the flame stabilization mechanism in the secondary stage [7,8]. Multi-nozzle, premixed arrays have been investigated by several academic and industrial groups characterizing emissions, thermoacoustic instabilities,

* Correspondence to: 1200 Montreal Rd., Ottawa, Ontario, Canada.
E-mail address: Patrizio.Vena@nrc-cnrc.gc.ca (P. Vena).

https://doi.org/10.1016/j.jaecs.2024.100260
Received 2 August 2023; Received in revised form 6 February 2024; Accepted 3 March 2024
Available online 11 March 2024
2666-352X/© 2024 Published by Elsevier Ltd. This is an open access article under the CC BY-NC-ND license (http://creativecommons.org/licenses/by-nc-nd/4.0/).

Nomenclature

Roman letters

AM	Additive manufacturing
D	Nozzle diameter m
DP	Differential pressure
F	Frequency Hz
FFT	Fast-Fourier transform
FOV	Field of view
MFR	Micromix-fuel ratio
PT	Pressure Transducer
P	Pressure kPa
P_y	Primary fuel channel
S_y	Secondary fuel channel
U	Inlet velocity m/s
$\dot{V}$	Volumetric flow rate SLPM

and operating conditions for these multi-element systems that are prone to flame–flame interactions [9–12]. Micromix systems have recently received renewed interest to perform premixed, or partially-premixed, combustion through the rapid mixing of small fuel jets [3,13–16]. This was made possible with the growing use of additive manufacturing in combustion system design [17–20] that enabled the design of novel geometries with complex, miniaturized, internal fuel passages to deliver the fuel at the desired location to realize compact micromix injectors.

The micromix concept relies on miniaturized, distributed fuel injection to answer the shortcomings of the premixed technology for fuels with a high-hydrogen content [3]. Instead of having a premixed fuel and air mixture flowing through the injector body to, ideally, achieve a perfectly-premixed, uniform mixture out of the injector, the fuel is injected near the exit of the injector and is rapidly mixed with the incoming air. This may result in non-premixed, or partially-premixed, combustion modes, depending on the overall design and operating conditions. While various injection strategies may be used to achieve efficient mixing, the injection through small jets in crossflow has garnered more interest [13–15]. This injection strategy ensures that flashback, as defined traditionally, cannot occur since no reactive mixture, through which a flame could propagate upstream, is present in the injector body. Additionally, the miniaturized flames, which result in shorter residence times through hot regions of the flow, have the potential to produce less thermal-NO than comparable premixed systems with longer flames [13]. These two critical advantages over premixed combustion systems have been demonstrated for high-hydrogen content fuels with acceptable levels of pollutant emissions in various combustion systems at different operational scales in experimental setups to small demonstration plants [3,14,21].

While the micromix combustion concepts are adequate for high-hydrogen content fuels, they only offer limited fuel flexibility for hydrocarbon blends. Stable operation has been observed down to 60% H_2 content in the fuel [15], which already provides considerable range in fuel flexibility. However, the widespread use of hydrogen, or the implementation of the hydrogen economy, for energy production remains a distant objective [22]. Consequently, micromix combustion systems can only have a limited impact currently as they cannot burn current hydrocarbons and cannot be used to accelerate the transition to low-carbon fuels with smaller hydrogen fractions. Fuel flexible energy systems that can accommodate current hydrocarbon fuels, pure hydrogen, and any blends of the two would provide significant advantages towards the implementation, and rapid adoption, of low-carbon fuels with increasing hydrogen content as they become available.

Towards this goal, a novel preliminary premix/micromix injector configuration was recently introduced [16]. The injector relies on a primary fuel injection in a premixed mode with a secondary fuel injection in a micromixed mode. By controlling the primary/secondary fuel ratio, stable flames were obtained at atmospheric pressure conditions from pure methane to pure hydrogen with a single burner geometry. While promising results were achieved for a single nozzle, practical systems are made of several such compact injectors distributed in complex arrangements. The impact of flame–flame interactions in these multi-element systems has seldom been studied for traditional premixed configuration [9,10,23–26]. While these previous studies cover significantly different operating conditions and burner geometries, they share the same conclusions that the impact of neighboring flames affect significantly the combustion behavior and dynamics. For premix/micromix combustion, understanding the stabilization mechanisms in stratified reactive mixtures becomes crucial to avoid flame merging that might lead to hotter regions in the flow, from locally richer reactant mixtures, with longer residence times that are detrimental to NO_x emissions and as well as understanding the impact of the different combustion modes on stability margins.

The current work uses a 5-nozzle array positioned in a cross pattern to evaluate the impact of a multi-nozzle configuration of the novel premix/micromix concept. The array is installed in the Atmospheric Combustion Rig at the National Research Council (NRC) Canada which provides visual access to the 5 flames to perform laser diagnostics. The stability and combustion dynamics maps are obtained for pure hydrogen fuel and compared to the single nozzle geometry [16]. OH planar laser-induced fluorescence (PLIF) is used to characterize the different flame shapes, and the measurements are temporally registered with the acoustics signals to obtain phase-averaged sequences. This dataset provides insight into the combustion process of the premix/micromix burners when placed in an array to better understand the challenges associated with this novel fueling strategy towards a rapid transition to sustainable fuels.

2. Methodology

2.1. Micromix, 5-nozzle array combustor

The Atmospheric Combustion Rig, shown in Fig. 1, at the NRC [17,27] was recently instrumented with acoustics sensors for the characterization of the single nozzle micromix injector [16]. In this work, a new combustor test section is introduced to accommodate the larger 5-nozzle array base plate. The combustor is designed to maintain the same internal aspect ratio as the smaller version used in single nozzle experiments [16]. This larger combustion chamber has two pairs of different fused-silica windows as can be seen from the front (Fig. 1a) and side (Fig. 1b) views of the rig. The larger windows are used for the imaging side of the optical diagnostics and provide complete optical access to the combustor and could be used to perform flame-wall interaction studies under confined conditions, outside the scope of this work. The 5-nozzle array is oriented in a cross pattern (Fig. 1c), where the laser sheet cuts through the three nozzle centerlines. The inlet nozzles 1–3 have the same clocking of injection holes, while nozzles 4 and 5 are rotated 180°.

The complex geometry of the premix/micromix injectors with miniaturized internal fuel passages is made possible through the use of additive manufacturing. Individual injectors were printed out of Inconel 625 on EOS M290 machines using laser powder bed fusion (L-PBF) [28], where a typical surface roughness of 5–20 μm and 40–80 μm is achieved for supported and unsupported structures, respectively. The nozzles generally have material properties better than cast parts and similar to forged ones. Additional machining is performed on external surfaces that mate with other components, such as the fuel plenum or the 5-nozzle array dump plate. Visual inspection is conducted to remove injectors with obvious defects from testing while effective area measurements are performed to assess the quality of printing on the micromix channels and openings across the different

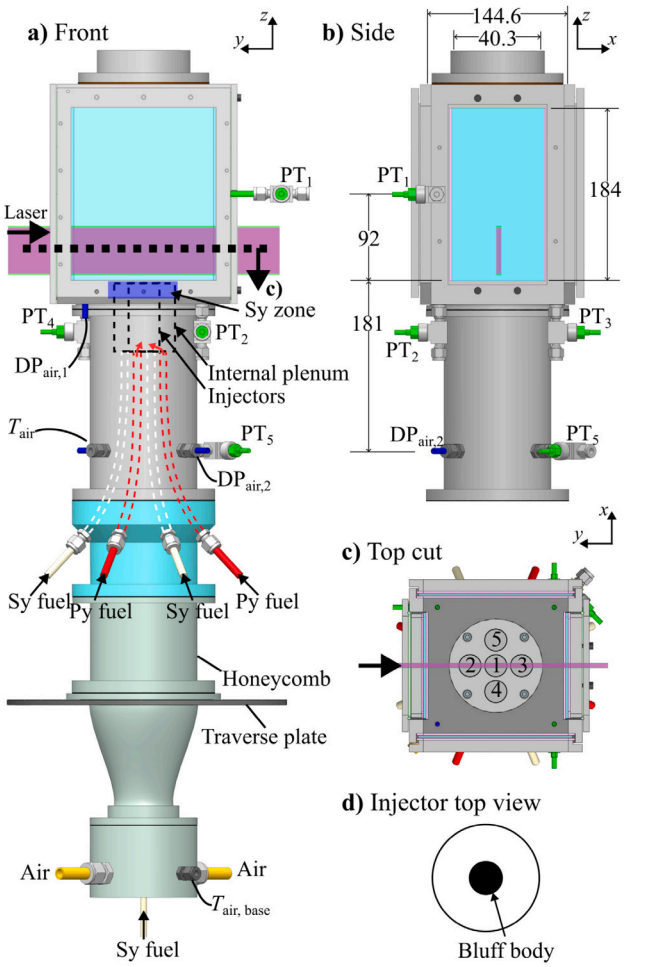

Fig. 1. (a) Front view of the Atmospheric Combustion Rig for the 5 nozzle-array with instrumentation. (b) Side view of the air plenum and combustor. (c) Top cut view of the combustor showing the nozzle arrangement in the 5-nozzle configuration. Note that the square shaped combustor is designed with large and small windows facing the front and side views, respectively. (d) Top view of the injector highlighting the bluff body at the center of the burner. Dimensions are in millimeters.

prints. The injectors selected for testing had effective areas measured within ±4% for the air and fuel channels.

The premix/micromix injector relies on a two-staged fuel injection strategy. Primary fuel injection is performed sufficiently upstream of the nozzle exit to achieve a premixed mixture in the injector body, and secondary fuel injection follows the micromix strategy of injecting fuel through multiple small jets in crossflow near the injector exit. Reactant air enters the base of the burner and flows through expanding and honeycomb sections. The air then continues through the air plenum and premixes the fuel at the primary injection site before flowing through the injector through a swirling section. The fuel for both stages is delivered through the air plenum using 8 mm nylon tubing via bored-through Swagelok fittings shown in Fig. 1a which connect to the internal fuel plenum. In the 5-nozzle array, each injector has a dedicated secondary fuel line (5) going directly to the injector, and 4 primary fuel lines distribute the fuel across the injectors in the internal fuel plenum. This results in 9 flexible tubes passing through the air plenum. Multiple premix and micromix fuel holes are distributed across the injector to provide adequate mixedness and uniformly distributed fuel injection, respectively.

Reactant H_2 and air flows are controlled using Brooks thermal mass flow controllers (MFC) (SLAS58000 Series), calibrated by the supplier. Two sets of MFCs are used in the experiments to provide better accuracy across the broad range of flow rates studied. For hydrogen, smaller 80 SLPM MFCs are calibrated with an accuracy of ±0.2% of the full scale (F.S.), while larger 1200 SLPM MFCs achieve ±1% F.S. For the air flow, a 1500 SLPM and 2500 SLPM MFCs both have an accuracy of ±1% F.S. The air flow is provided by a compressor (Sullair 4509AC) and limits the maximum flow rates up to ~2500 SLPM in the current setup. The operation of the Atmospheric Combustion Rig is performed using an integrated LabVIEW program. Flow parameters (inlet velocity and equivalence ratio) and the fuel split between the primary (Py) and secondary (Sy) fuel stages are controlled and monitored throughout the experiments. Primary and secondary fuel mixtures are controlled independently with dedicated MFCs to accurately control the fuel split between the premixed and micromixed modes, respectively. It is labeled Micromix-Fuel Ratio (MFR) which corresponds to the amount of secondary (micromix) fuel injection used with respect to the entire fuel delivered. The standard volumetric flow rates ($\dot{V}$) delivered through each channel are used to define the MFR in Eq. (1), where a MFR of 0 corresponds to a fully premixed mode, and a MFR of 100 to a pure micromixed mode.

$$\mathrm{MFR} = \frac{\dot{V}_{\mathrm{Sy}}}{\dot{V}_{\mathrm{Py}} + \dot{V}_{\mathrm{Sy}}} \tag{1}$$

The air and external fuel plenums and the combustion chamber are instrumented with pressure ports connected to differential pressure (DP) transducers (Yokogawa EJX110 A and Rosemount C1151DP), achieving a 0.25% accuracy on the full scale, and type-K thermocouples. The effective area of each passage is measured with these sequentially for the air passage and the primary and secondary fuel channels with cold air. These measurements are repeated daily to check the integrity of the complex miniaturized fuel channels and ensure a consistent setup (within 5% variation) when using different injector prints. This is crucial to ensure that the hardware has not been damaged, especially after repeated flashbacks during the stability mapping, since the internal channels are not visually accessible for inspection. The daily checks are performed for individual passages at three flow conditions and achieve a standard deviation of the mean of less than 2% for each flow path for the ensemble of hardware configurations tested. During the experiments, the fuel and air flow properties are monitored and the momentum flux ratio through the micromix injection as jets in crossflow is calculated using the integrated LabVIEW program.

Acoustics measurements are performed using five acoustic pressure transducers (PT, PCB Piezotronics pressure sensor, ICP model 112A22) achieving a resolution of 0.689 Pa. They are mounted with semi-infinite coils (l = 5 m, outer diameter 1/8" X 0.030" wall). Four of them, PT_1–PT_4, are installed on the combustion chamber as shown in Fig. 1a–c. PT_1 is mounted at mid-height of the combustion chamber and PT_2–PT_4 are located in the corners of the combustor base. The fourth corner is used to measure the differential pressure between the combustor and the air plenum. The fifth transducer, PT_5, is mounted on the side of the air plenum. Distances between the sensors are given in Fig. 1b. The pressure traces and the frequencies obtained from the fast Fourier transform (FFT) of the previous 1 s of measurements are monitored continuously throughout the experiments and acquired at a sampling rate of 25.6 kHz. This ensures that the system can acquire the principal longitudinal mode, expected to appear in the 600 Hz frequencies, and higher-frequency modes present in noisy conditions with multiple flames. The acoustic data acquisition is performed with an stand alone LabView program and a different computer than the one used to operate the rig. In addition to the 5 signals of the PT, the system acquires the laser Q-switch trigger, the Integrated Relay Optics (IRO) gate, and the sCMOS trigger used for imaging. Consequently, the laser diagnostics can be temporally registered with the acoustic measurements to provide phase-averaged PLIF measurements.

The burner is mounted on a three-axis traverse such that its position, with respect to the fixed laser sheets and cameras, can be moved to image different sections of the flame efficiently and position the field

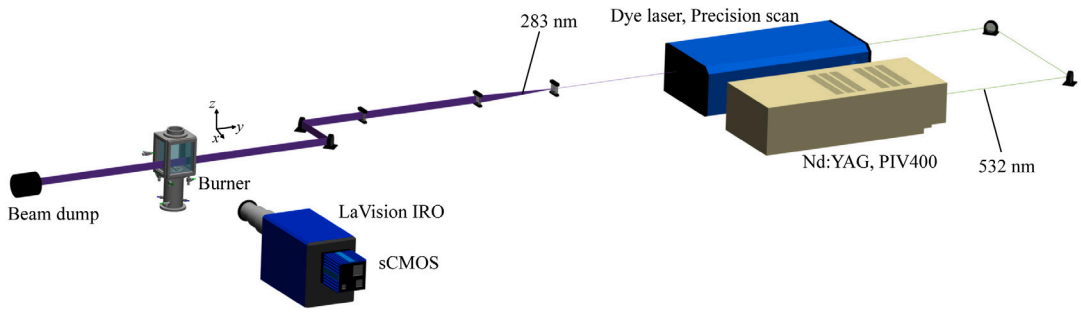

Fig. 2. Experimental configuration used in this work. Laser, IRO, and sCMOS triggers are acquired simultaneously with the acoustics data.

of view (FOV) of the flame to perform laser diagnostics. The z-traverse position is recorded for each condition to calculate the true height above the burner. During acoustic measurements, the traverse motors are shut off to mitigate noise leaking into the PT and turned back on to adjust the FOV at the next operating condition.

2.2. Diagnostics

The diagnostic setup is shown in Fig. 2 for OH PLIF. In this work, only the OH subset of the laser diagnostics discussed in detail by An et al. [17] is used. The ultraviolet beam (282.94 nm) is obtained by pumping a wavelength-tunable dye laser (Sirah, Precision Scan) using a solution of rhodamine 6G with the second harmonic of the Spectra-Physics Nd:YAG laser (Quanta Ray PIV400). The beam generated has an average output energy kept between ~4.5–5.5 mJ/pulse to ensure measurements are performed in the linear LIF regime [17]. The energy output is adjusted while the flame is running as the acoustic waves are affecting the energy measurements performed without a flame. The beam is formed into a thin, slightly diverging, laser sheet, approximately 60 mm tall in the region of interest. It is centered above the three nozzles centerline axes, as shown in Fig. 1c.

The OH PLIF images are acquired using a sCMOS camera attached to a IRO (LaVision Intensified Relay Optics). The fluorescence signal is collected by the IRO, equipped with a bandpass filter (320±20 nm), with a gate time of 150 ns and a gain of 55% of maximum. The raw images are corrected for pulse-to-pulse laser energy variations and mean laser profile. The laser profile is obtained by generating a uniform acetone field prior to the experiments. For these experiments with multiple flames in the laser path, non-uniform OH PLIF signal are still obtained after normalization, as seen in other work [25], due to difference in absorptivity between OH and the acetone tracer used to measure the beam profile. The spatial calibration is performed with a millimetric grid, resulting in a FOV for the LIF measurements that covers an area of approximately 110 mm × 60 mm (width × height). The sCMOS camera captures the intensified signal with a spatial resolution of 57.3 μm/pixel. The PLIF and laser system are triggered synchronously using a LaVision timing unit and 520 images per set are acquired at a frequency of 10 Hz.

2.3. Phase registration of laser diagnostics

The IRO gate signal is used to register the laser diagnostics temporally. The process is shown in Fig. 3 for a relatively quiet condition. For clarity, only two acoustic signals and the IRO gate signal are shown in Fig, 3a, but the acquisition is done simultaneously for the 5 pressure transducers and the 3 laser/camera signals. In this case, the reference signal used to register the laser diagnostics is obtained from PT_1 located at mid-height of the combustor. The 1 s sequence shows the expected 10 gates from the laser diagnostics. The peak signal is used to register the fluorescence image.

The beginning of the acoustic cycle ($\theta = 0°$) is defined by the zero-upward crossing location. The phase at which the OH PLIF image is acquired can then be readily calculated over the complete single cycle

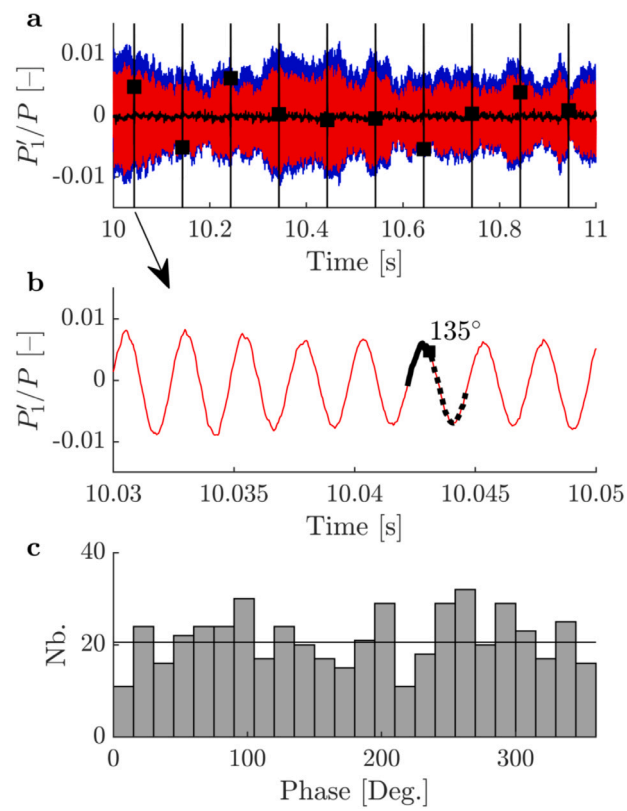

Fig. 3. Example of phase registration for the MFR100 and U_{in} = 20 m/s condition. (a) Pressure trace shown for PT_1 (mid-height) and PT_2 in red and blue, respectively. The IRO gate is shown in black with symbol corresponding to the location where the frame is acquired. (b) The phase is identified from the zero-upwards crossings and used to register the phase location of the laser diagnostics. (c) Distribution of the acquired frames using 15° phase bins.

in which the image is acquired, as shown in Fig. 3. The entire dataset can then be distributed in phase bins to group PLIF images with similar acoustic phases and perform phased-averaged analysis. In this work, 15° bins are selected. They provide an adequate phase resolution to observe the flame motion while having a reasonable number of frames per bin, typically around 20, and an even distribution of frames per bin as shown in Fig. 3c.

2.4. Operating conditions

This work focuses on operating the premix/micromix injector with pure hydrogen. The fuel-air ratio is maintained constant for all the MFR conditions to achieve a globally-lean mixture with an equivalence ratio of ϕ = 0.61 and a target adiabatic flame temperature of interest for gas turbine applications. The stability map is performed in increments

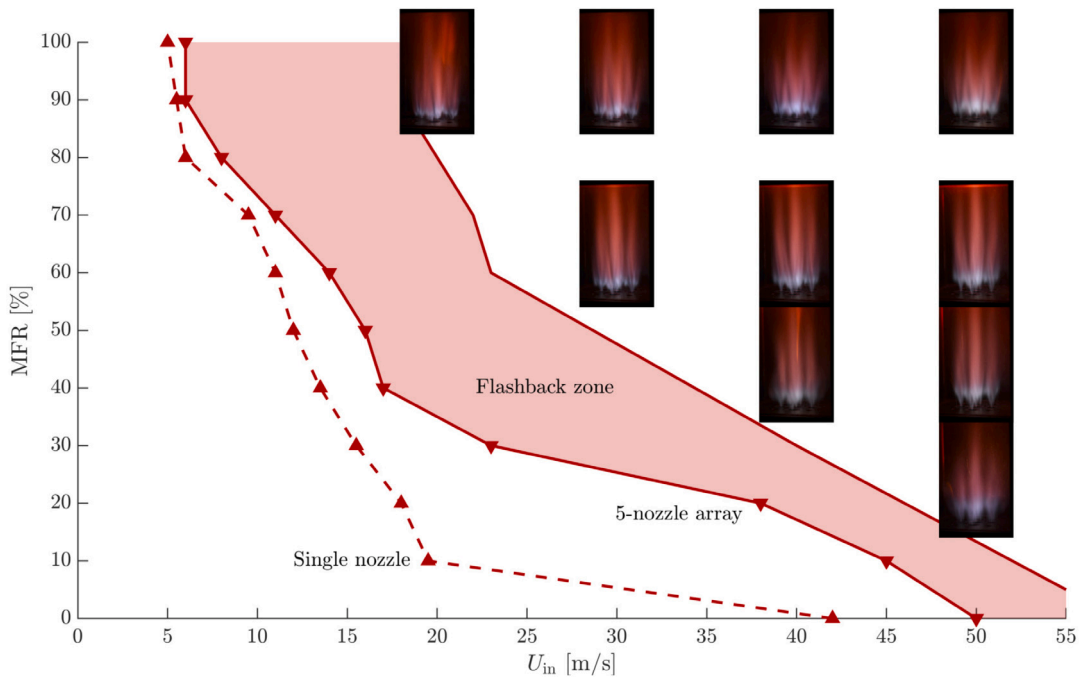

Fig. 4. Stability map for the 5-nozzle array shown by solid lines. The flashback limit for the single nozzle is shown as a dashed line for comparison. A flashback zone was observed for the 5-nozzle array depending on the nozzles used in the array and the orientation of individual injector. Blowoff could not be achieved with the experimental setup due to limitations in the flow rates delivered by the compressor.

of 10% MFR covering the entire range from fully-premixed, when possible, to fully micromixed operation.

To measure flashback/blowoff velocities, the bulk inlet velocity is gradually reduced/increased from a stable condition. The definition of the lower operability limit, known as the flashback limit in premixed systems, is adjusted in this work as flames with larger micromix fractions do not result in traditional flashback where the flame would propagate into the injector. Here, the operability limit is identified when either conventional flashback or overheating of the injector is observed. For conventional flashback observed in premixed dominated conditions, the flame rapidly propagates upstream into the injector. For the predominantly micromixed conditions, overheating of the injector occurs and the hardware starts glowing if the flame sits too close to the nozzle exit. While the micromix approach is designed to remove the risks of conventional flashback for high-hydrogen content fuels, the heat from the flame can still be transferred to the hardware at low enough velocity, or if the hydrogen flame attaches to surface defects. Even if the flame does not propagate into the injector, significant hardware damage can occur for prolonged operation in this regime.

3. Results

3.1. Stability map

The stability map obtained for the 5-nozzle array is presented in Fig. 4 with a selection of visible emission pictures captured with a Nikon D750 (f/5.6, 1/25 s, ISO-3200) camera. In low light, the flame chemiluminescence appears as a faint white on the camera with some red and near-infrared radiation from water captured by the camera in the post-flame region [29]. Blowoff could not be achieved for any of the fuel split conditions. Limitations on the maximum flow rate delivered by the compressor kept bulk inlet velocities to below 60 m/s, such that the stability map focuses on the flashback limit and compares the flashback velocities for the single nozzle reported in Durocher et al. [16].

A rapid inspection of the chemiluminescence pictures presented in Fig. 4 highlights that there are only limited changes in flame structure across most of the conditions. Except for conditions near the stability limit and for high premixing fractions (MFR≤30), the majority of the flames exhibit a compact flame structure close to the injector exit. Unstable conditions at lower MFR produce flames that are showing significant displacement, as demonstrated by the blurred flame brush at MFR30.

The lower operability limit for the 5-nozzle array has been performed for two injector configurations. Several additively manufactured injectors were received and tested. An ensemble of prints were selected from visual inspection to remove those with visible defects and through effective area measurements to promote, as much as possible, a consistent set of injectors to be installed in the rig. Through testing of different configurations, a flashback zone is reported in Fig. 4 where flashback velocities are measured as soon as a single nozzle of the array flashes back. This zone indicates systematic variations between injector configurations that lead to variations in operability limits. In the optimal configuration, lower flashback velocities were achieved across the entire operating fuel split. In contrast, some printed injectors, with no visible defects, provided flame anchoring points on the injector hardware for the hydrogen flame to propagate upstream, either through the injector achieving traditional flashback or overheating of the hardware. An important variability is observed here for hydrogen fuel with the most significant span in flashback velocities observed for the micromix combustion mode (MFR100), where the flashback velocities increases by ∼200% from the optimal condition. The changes in flashback limits with a different configuration of injectors highlight the importance of consistent designs for additively manufactured injectors. Understanding the impact of partially-premixed and micromixed combustion in multi-nozzle combustion systems operating with highly reactive fuels such as pure hydrogen becomes crucial for the deployment of such technology. In these systems, a single localized flame flashing back in a large array containing tens of injectors could provide an anchoring point for the hydrogen flames, potentially resulting in hardware failure if not identified in time.

For either configuration studied, the flashback limit follows a slow increase in flashback velocity from the micromix operation (MFR100) to partially-premixed conditions (MFR50-60) and a rapid increase in

flashback velocity towards the premixed condition (MFR0). For the higher MFR case, flashback generally occurs on the same nozzle as the flame anchors on the hardware. The flashback mechanism differs for the low MFR cases. In these conditions, there is often large flame flapping/oscillating that may lead to any one of the nozzles flashing back if the appropriate flow conditions are met locally. These more premixed cases have significantly louder flashback than for the micromixed dominated conditions.

The flashback limit obtained for the single nozzle configuration with the optimal print [16] is also compared to the 5-nozzle array. For higher MFR, the single nozzle has slightly lower flashback velocities compared to the optimal 5-nozzle array configuration. Once placed in the array, defects in other nozzles and the hot boundary condition seen by the flames, due to adjacent flames, both contribute to the higher flashback velocities in the array. For the lower MFR conditions, a larger difference is observed between the single nozzle configuration and the array. In these conditions, larger pressure amplitudes are measured in the combustor in the presence of flame–flame interaction. With 5 nozzles under larger thermoacoustic perturbation, the probability of flashback through a single injector is increased due to the stochastic nature of flashback, and higher local velocities are therefore needed in the array to be within operational limits.

3.2. Instantaneous OH-PLIF

Laser diagnostics are performed for the 10 conditions presented in Fig. 4 with chemiluminescence pictures. The experimental points cover MFRs of 100, 70, 50, and 30. Completely premixed pure hydrogen flames could not be stabilized on the 5-nozzle configuration as flashback would occur at the maximum bulk velocity possible with the compressor. As these partially premixed flames have non-axisymmetric structures [16], the OH-PLIF obtained from the sheet crossing the centerline axes of the injectors can be difficult to interpret. Here nozzles 1–3 are identically clocked such that every nozzle investigated with the laser system have the same orientation leading to similar features expected to be present in similar region above each nozzle. The other two nozzles (4–5) out of the planar diagnostic have a different orientation and are rotated by 180°.

A comparison of instantaneous OH-PLIF frames is provided in Fig. 5 for decreasing MFR values at a constant inlet velocity of 50 m/s. Wrinkled lifted and attached flames are observed throughout the entire dataset for this globally lean hydrogen mixture. Increasing OH signal is measured in the wake of the bluff body for conditions with a higher micromix fraction in contrast to the predominantly premixed flame (MFR30) where a weak signal, if any, is observed. For the high micromix fraction, mixing with the fuel jet occurs rapidly and distributed combustion occurs not only in the outer sheer layer, but also behind the bluff body.

Instantaneous OH-PLIF images show the impact of increasing bulk inlet velocity on the micromix combustion mode in Fig. 6. Similar patterns in the OH-LIF signal are observed with wrinkled flame structures and distributed combustion zones. At lower velocity (Fig. 6a), the three flames are strongly attached in the recirculation zone behind the bluff body. They do not appear to be interacting as distinct flame fronts are observed for each injector. As the inlet velocity increases, the flames are gradually lifting from the nozzles and exhibiting more pronounced wrinkling. The lifted flames suggest that the momentum of the jets-in-crossflow is enough to push the flame further downstream in the wake of the fuel injection, thus promoting mixing with the incoming air. Consequently, there appears to be a more uniform combustion zone located 3 diameters downstream of the nozzles as the hollow core in the wake of the bluff body gradually disappears. Flame interaction also appears at higher inlet velocity as the distinct flame fronts observed at lower velocity now merge and result in zones with strong OH signal between nozzles.

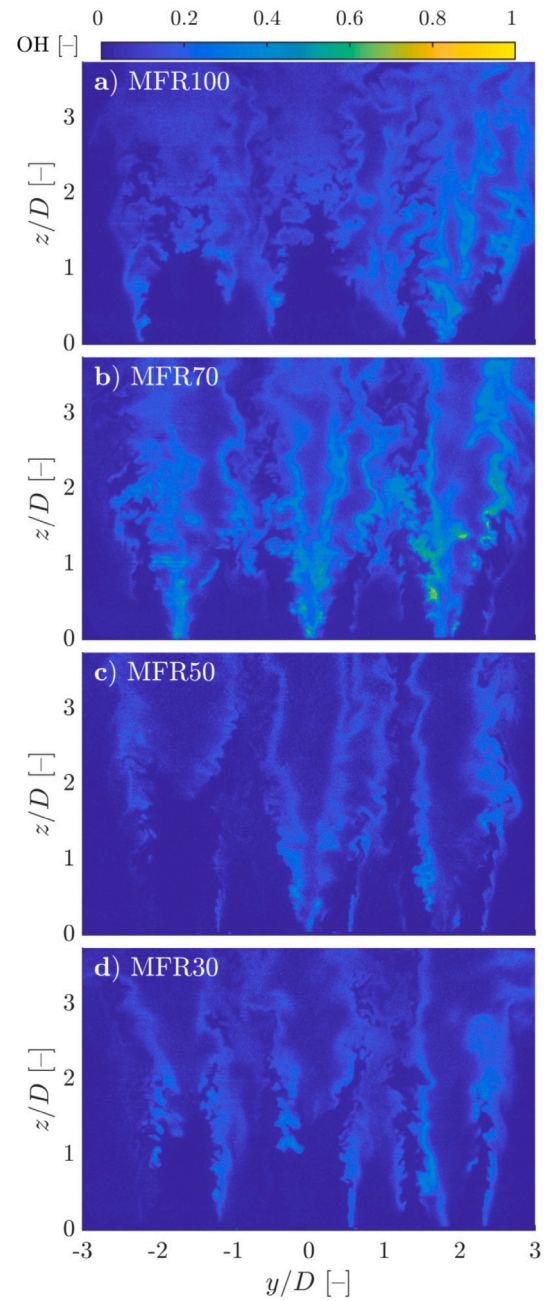

Fig. 5. Instantaneous OH-PLIF field for conditions with an U_{in} = 50 m/s and MFR of (a) 100 (micromixed), (b) 70, (c) 50, and (d) 30.

3.3. 3D OH-PLIF reconstruction

While the OH-PLIF slice across the nozzle centerline provides valuable insight into the combustion process of this multi-nozzle array, the nature of the micromix concept makes it difficult to get a complete understanding of the flame structures from a single laser sheet. Contrary to premixed combustion systems where fuel is generally distributed uniformly and leads to axisymmetric flame structures, these partially-premixed and stratified flames have highly three-dimensional structures. The localized injection of fuel as jets in crossflow also implies that there might be pockets where no combustion occurs in between fuel injection locations.

To gain better insight into the complex structures of these flames, a three-dimensional (3D) OH-LIF volume is reconstructed from multiple

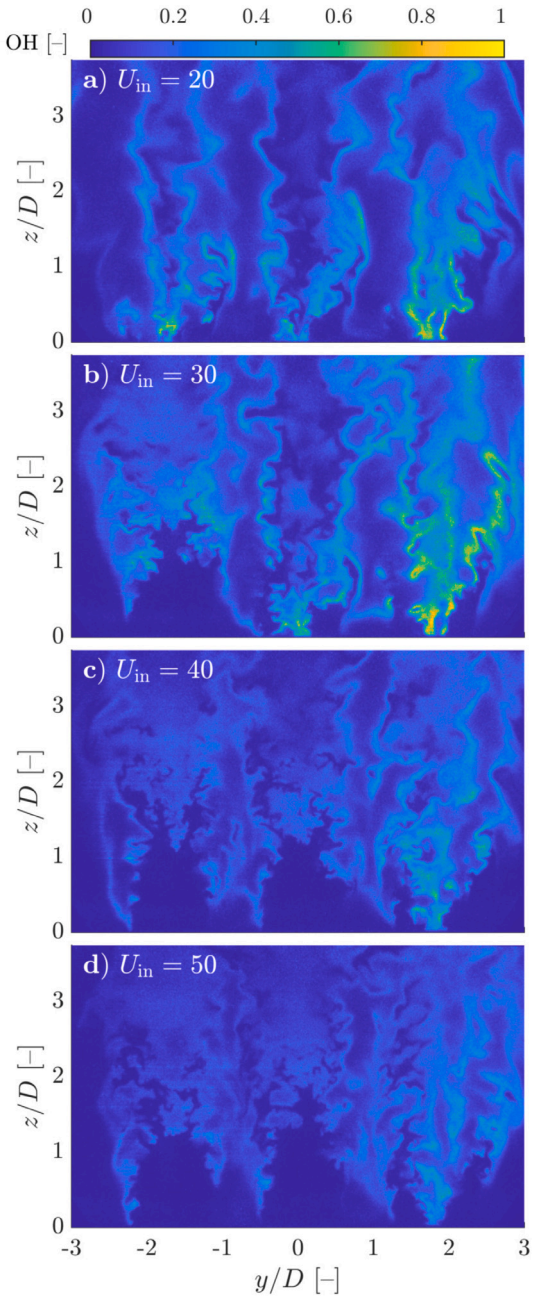

Fig. 6. Instantaneous OH-PLIF field for the fully micromixed operations (MFR100) with increasing inlet velocities (U_{in}) of (a) 20, (b) 30, (c) 40, and (d) 50 m/s. The color scale is consistent with Fig. 5.

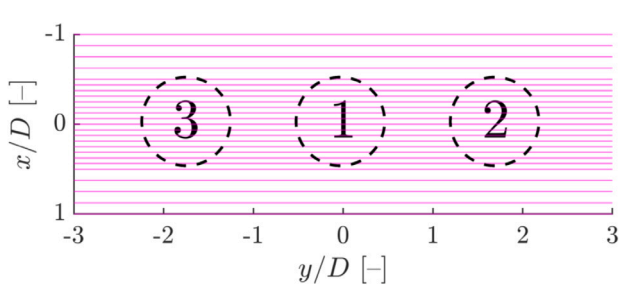

Fig. 7. Spatial resolution of laser slices performed to reconstruct the 3D mean OH-PLIF field. The nozzle location is given by the black dashed circles. The laser sheet enters from the right (positive y) and exits to the left (negative y).

OH-PLIF datasets acquired at different x positions. The x-traverse is moved at 25 distinct x/D locations shown in Fig. 7, where datasets with 520 images are acquired at each location. The average OH-PLIF field is obtained for each location and normalized by the mean laser energy. The 25 sets are then assembled to produce the reconstructed OH-LIF volume.

Fig. 8 provides an example of the mean OH-PLIF field (Fig. 8a) and the reconstructed horizontal fields (Fig. 8b–d) that are obtained at different heights above the burner (HAB). The nozzle locations are indicated by dashed circles on the reconstructed images for reference. This condition corresponds to a relatively quiet case at a MFR100 and $U_{in} = 20$ m/s. As such, the injectors are operating in fully micromixed mode, leading to non-uniform and non-axisymmetric flames. The horizontal reconstructions on the xy plane clearly show localized flame structures that would otherwise be imperceptible on the OH-PLIF images along the original vertical $z - y$ plane. While the 2D field does provide meaningful information to better understand the stability mechanisms for this premix/micromix injector concept, a thorough characterization of the combustion properties will require challenging diagnostics to effectively capture the three-dimensional (3D) structures observed.

The mean, reconstructed OH fields are shown for a sequence of increasing heights above the nozzle exit in Fig. 9 up to $2D$ downstream of the injector exit. The same color scale is applied through the entire sequence with the laser entering the FOV from the right side of each frame (positive y/D). Even with the laser beam profile normalization, the right flame still shows a stronger signal. This stronger OH-LIF signal results from the laser attenuation through the inline flames and has been seen previously for laser diagnostics in linear arrays [25]. This results in larger signal intensities on the flames closer to the laser source and does not imply a higher combustion intensity of the flame. Many interesting features are observed from the slices taken at different HAB in the reconstructed OH volume. As mentioned previously, the use of micromixing with discrete, localized fuel injection results in non-axisymmetric, 3D flame structures. In addition, flame structures vary locally throughout the 5 nozzle cluster, as the three-dimensional flame branches of the central nozzle, which entrain hot or reactive mixture from the neighboring nozzles, differ from those of the outer nozzles that entrain cold air. This is a marked difference from traditional premixed burners used in gas turbines and provides new challenges for diagnostics in partially-premixed combustion to better understand this type of injector. The orientation of each nozzle with respect to one another and the overall orientation of the array cut by a single vertical laser sheet have to be carefully selected to perform diagnostics. In this work, the localized fuel injections were used as markers to position the nozzles such that the three in-line with the diagnostics would face the same direction with the other two nozzle outside the measurement plane rotated by 180°. The injector clocking becomes an additional design parameter to be considered when setting up multi-element arrays using micromixed combustion strategies. The distributed fuel jets lead to localized flame structures that can be more prone to flame merging if neighboring fuel injections intersect.

The flame petals, also observed visually in the single nozzle configuration [16], become clearly visible with the slices in the x–y plane presented in Fig. 9. It appears that the central nozzle has closed flame petals where the outer localized flames appear open. Focusing on the central injector, located at $y/D = 0$, the three lobes appear to be strongly attached behind the bluff body and more weakly to systematic locations on the interior lip of the injector exit. The flames gradually connect at larger HAB (Fig. 9d) resulting in three oval-shaped structures before expanding again and leaving a non-reacting core in the wake of the bluff body (Fig. 9f). A minor counterclockwise swirling motion is observed from these frames within $1D$, but it rapidly becomes indiscernible further downstream of the nozzle where the flame structures mainly follow the axial direction of the flow towards the combustor exit.

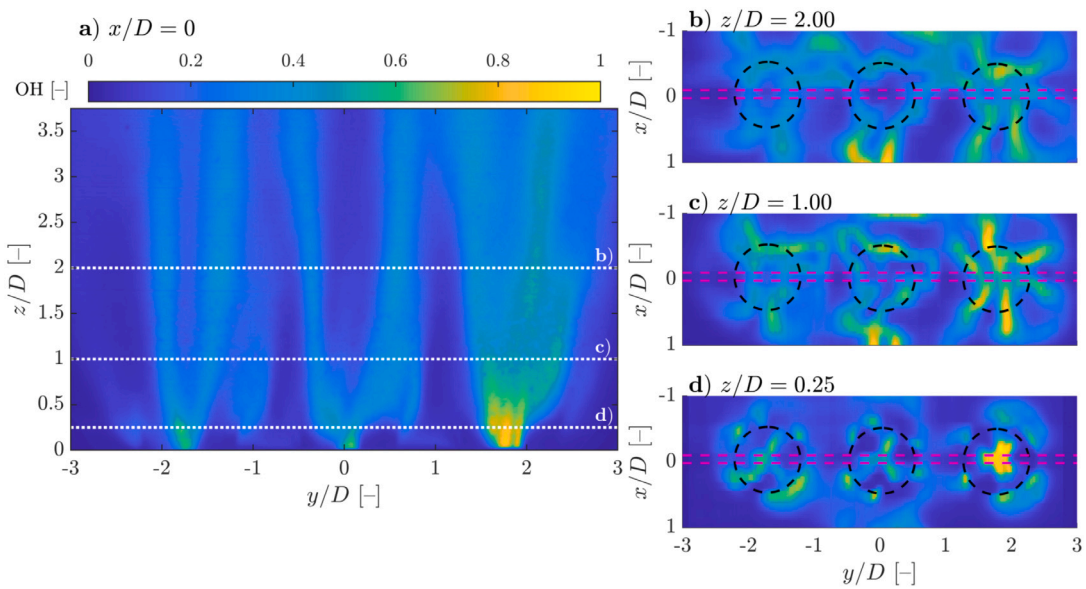

Fig. 8. (a) Mean OH-PLIF field along the nozzle centerline ($x/D = 0$). The white dotted lines correspond to the HAB (z/D) at which the assembled cross-sections of mean OH-PLIF are shown in b–d. The laser sheet location is shown between the dashed lines. A larger thickness is shown for clarity.

Similar structures are observed on the outer injectors, but with the flame petals mostly open. Since these injectors were installed with the same orientation, a similar distributed flame shape was initially expected. For most of the localized flame structures, however, this configuration leads to six distinct flames. This star pattern is more visible on the right injector ($y/D \approx 1.8$) at smaller HAB, while some of the flame petals on the left injector ($y/D \approx -1.8$) appears to be closed. It is important to note that injectors 4 and 5 outside the laser planes are clocked in a different orientation (+180°) from the three inline nozzles 1–3. In this orientation, micromix jets from nozzles 4 and 5 occur towards localized fuel injections from the rightmost injector. That could potentially lead to the jet merging and creating the open flame branches observed. For the central and left injectors, marginal fuel jet merging should occur from neighboring injectors leading to the mostly closed flames.

The horizontal slices show that combustion is happening in between injectors. From Fig. 9a–g, a faint OH signal is captured between the open flame petals stabilized on the right injector with the central injector and eventually with the two injectors outside the region of interest scanned with the laser ($x/D < -1$ and $x/D > 1$). For these multi-nozzle systems, such interactions between injectors can lead to more complex flame–flame dynamics and undesired behaviors.

Flame merging is observed in these frames. The localized flames on both the central and bottom injectors ($x/D > 1$) are initially distinct, but merge starting from an HAB of approximately 1 D (Fig. 9i), leading to two strong flame fronts further downstream of the nozzle exit (Fig. 9l–n). Such behavior leads to strong combustion in these regions with well-anchored flames in the merging flows. The resulting hot regions are elongated, stretching for more than 1 D. As such, these can potentially support stronger thermal-NO formation and overall poor emissions characteristics. For these micromix systems, it has generally been recommended to avoid flame merging because of the detrimental impact on emissions [3].

Achieving such conclusions would not be possible using only single OH-PLIF frames. The complexity of the non-axisymmetric, 3D flame structures highlights the need for 3D visualization techniques to fully understand the combustion characteristics of partially-premixed flames with micromix fuel injection. While 2D fields can provide insight into the combustion process, they could miss significant information to explain the stabilization mechanisms of micromixed flames. Tomographic OH measurements [30], or volume reconstruction from OH-PLIF, would be necessary to fully understand the complex behavior of these flames.

3.4. Combustion stability map

A combustion dynamics map was obtained for the 5-nozzle array using the PT_1 transducer, located at mid-height of the combustion chamber. Normalized pressure fluctuations (P_1/P) obtained from the pressure traces are presented in Fig. 10a and the dominant frequencies obtained through FFT are displayed in Fig. 10b. The acoustics signals are acquired during transient operation of the rig. A 120 s ramp is performed between two velocity conditions (horizontal bars), or two MFR conditions (vertical bars), and the acoustics are continuously acquired as the MFC are gradually, and autonomously, adjusting the air and fuel flows to maintain a constant flame temperature. The single-sided amplitudes are obtained over the domain using a 1s sliding window and only the maximum amplitude over the entire frequency domain is reported in Fig. 10.

Larger pressure fluctuations and noise are generally measured at low MFR and higher velocities for the 100% H_2 mixture. While this behavior is consistent with single nozzle experiments [16], higher pressure amplitudes are observed on average for the 5-nozzle array. The micromix fuel injection helps reduce the combustion noise by approximately one order of magnitude for pure hydrogen, when used in fuel splits over 70%. For these highly reactive mixtures, this range of MFR (70+) corresponds to the intended operation targets. The acoustics map highlights the important thermoacoustic behavior of premixed hydrogen flames in arrays. In addition to the higher flashback velocities, significantly larger pressure amplitudes, which may also contribute to a rapid flashback onset, are measured at MFR below 50%. For these predominantly premixed cases, large amplitude motions are observed in the axial direction of the combustor. In drastic cases, the flame may be pulsating in and out of some of the nozzles, eventually leading to flashback.

The singled-sided amplitudes shown in Fig. 10b highlight that the dominant frequency in most of the cases is found around 450 Hz. Other resonating peaks are generally found in the spectrum at higher frequencies, but only the dominant one is shown for clarity. A 3D Helmholtz solver (COMSOL Multiphysics® v5.6) was used to obtain resonances of the 5-nozzle array rig, without sources nor flow. The simulation assumes a homogeneous temperature in the combustion chamber and room temperature upstream of the injector. The entire Atmospheric Combustion Rig geometry is included in the model. An acoustically closed boundary condition ($u\prime = 0$) is selected at the base of the air

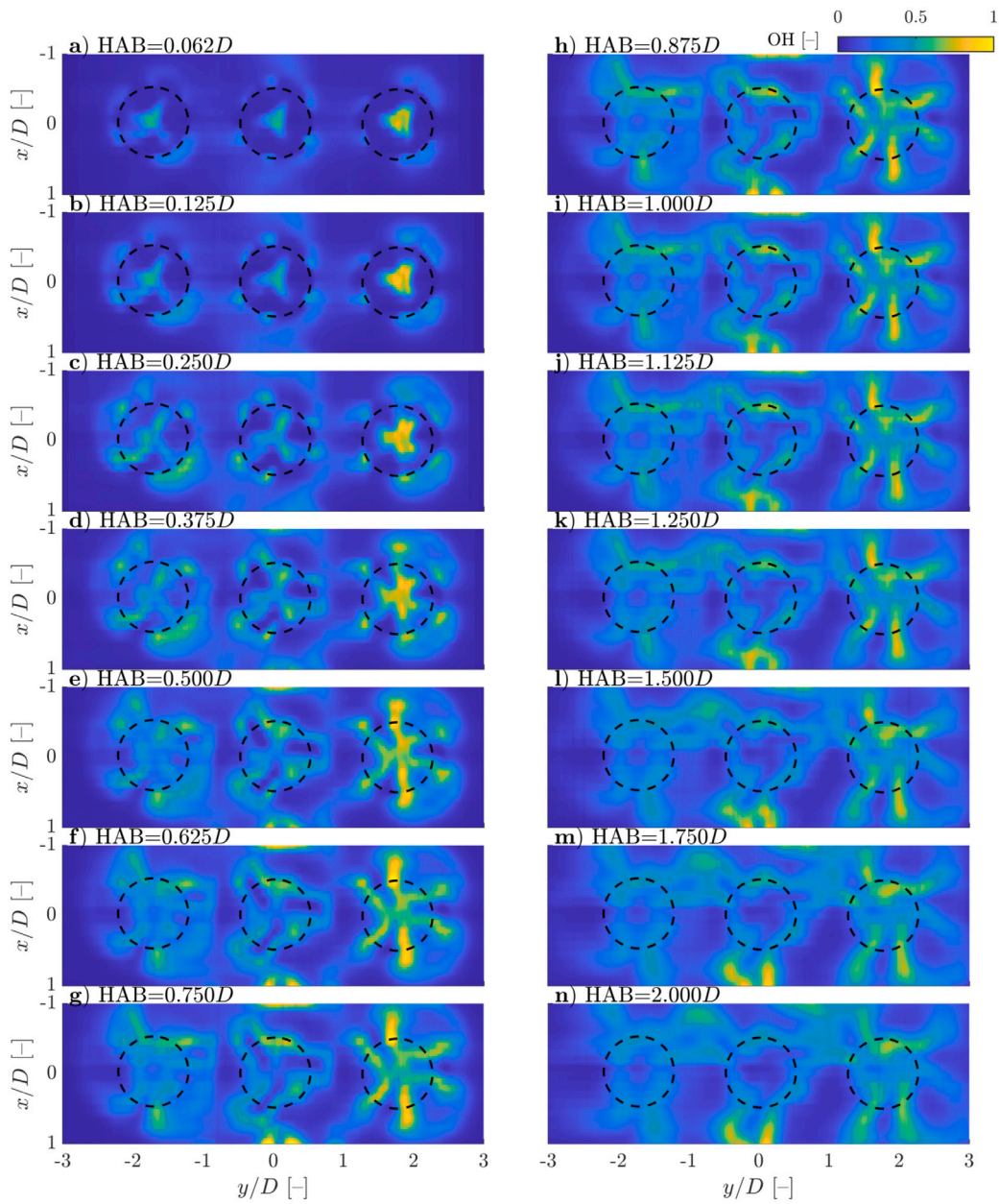

Fig. 9. Mean OH-PLIF fields obtained from horizontal slices through the reconstructed 3D field highlighting the non-axisymmetric behavior of the micromixed flame (100%H_2, MFR100, $U = 20$ m/s). The measurements are shown for increasing height above the burner (HAB) from (a)–(n). The nozzle locations are shown by the black dashed circles.

plenum and a radiative boundary is used at the combustor outlet to model the unflanged outlet. Acoustic monopoles with a conical shape, and centered on each injector centerline axis with the same phase are used as forcing sources. The monopole frequencies are swept from 5 to 10000 Hz and the resulting pressure fluctuation amplitudes, measured at the same location as the pressure transducers, are recorded as a function of frequency. The results show that the dominant frequency observed in the acoustics map at ∼450 Hz corresponds to a full wave through the Atmospheric Combustion Rig, from the air inlets to the combustor outlet (one wavelength). Since this wavelength is much larger than the axial length of the combustor, and that the combustor temperature varies minimally between conditions, it is expected that most cases presented in Fig. 10 exhibit a similar mode shape with frequencies close to 450 Hz.

At higher MFR, the longitudinal mode becomes less prominent in the frequency spectrum and higher frequencies at approximately 2700 Hz have similar single-sided amplitudes. It may even become the dominant frequency, as shown in Fig. 10b around 50 m/s and MFR90.

The complete frequency spectra are shown in Fig. 11 for the constant bulk inlet velocity of 50 m/s performed with decreasing MFR from 100% (micromix) to 0% (premix). A log-scale is used to provide better contrast between the resonant frequencies as the amplitudes observed at ∼450 Hz in predominantly premixed conditions are orders of magnitudes larger than other frequencies found in the domain. At lower MFR, the single-wave longitudinal amplitude dominates the frequency spectrum, but a range of higher frequencies is measured up to 10 kHz.

Significantly fewer resonant frequencies are observed for the larger MFR. In cases with MFR70+, the frequencies at ∼500 and ∼2700 Hz have similar single-sided amplitudes. As observed previously in Fig. 10b, around MFR90, the higher frequency can even become larger. For the partially-premixed mixtures, the flames start to anchor close to the secondary fuel injection holes, resulting in stratified combustion that appears to prevent the acoustic feedback through inhomogeneity in the local fuel-air mixture with different local equivalence ratios, and

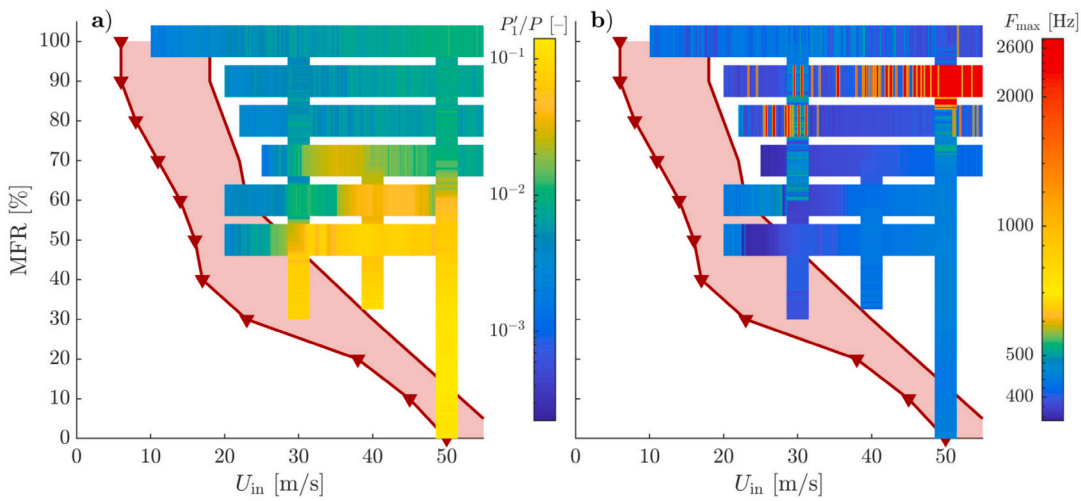

Fig. 10. Acoustics maps obtained for 100% H_2 showing (a) the maximum normalized amplitudes (P_1/P) measured with PT_1 and (b) the dominant frequency in the frequency spectrum. Note the log-scale on both figures.

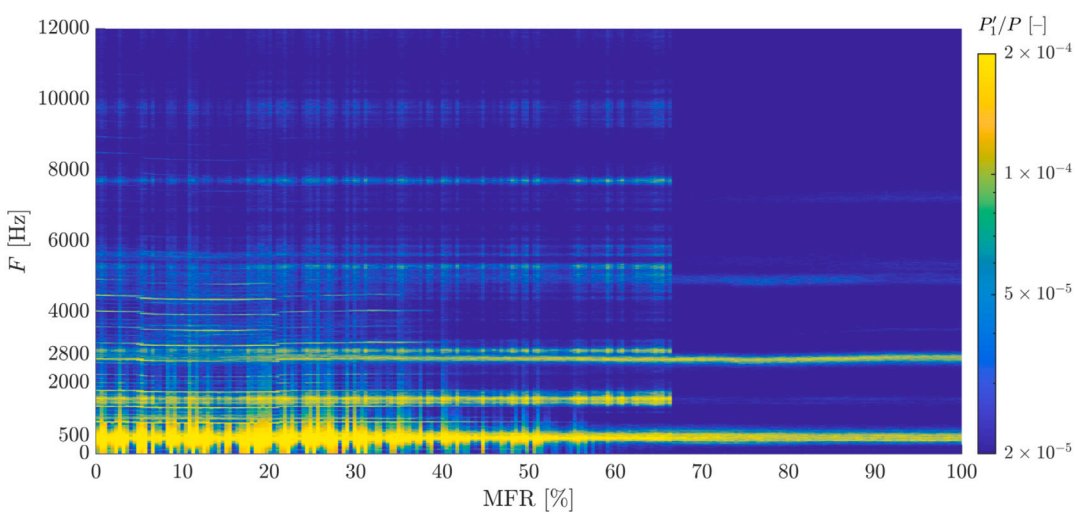

Fig. 11. Frequency spectrum obtained at $U_{in} = 50$ m/s. The measurements are acquired with PT_1. The single-sided amplitudes calculated with FFT are shown by the colorbar.

hence heat release rates. Additional modeling without homogeneous fields would be required to confirm that hypothesis.

3.5. Phase-averaged OH-PLIF

An OH-PLIF phase-averaged sequence is presented in Fig. 12 for the MFR30 and $U_{in} = 50$ m/s condition shown briefly in the instantaneous frames (Fig. 5d). It corresponds to an operating point where significant noise is measured with a marked dominant frequency at ~450 Hz. In this sequence, phase bins of 15° are used to perform the averages, and only every other bin is presented for brevity. An averaged cycle frequency of 458 Hz is measured from the cycles in which OH-PLIF frames are acquired. This corresponds to a combustion dynamic mode dominated by a single longitudinal full wave through the rig. In this sequence, only the right flame is attached to the bluff body at the centerline of the injector. The center and left flames have a lifted core with the flame edges attaching to the lip of the outlet of the injector. The lifted flames resemble a typical M-shaped flame, but characteristics of the micromixed, localized injection are observed even for this case at MFR30. Non-uniform flame structures are visible from this PLIF slice measured at $x/D = 0$, where stronger burning jets in the core region of the flame correspond to locally richer zones resulting from the mixing of the secondary fuel injection with the premixed mixture (from the upstream injection of primary fuel).

For the lifted flames, the approximate minimum and maximum location of the core are indicated by the red dashed lines. A motion of ~ $0.75D$ is observed in the acoustic cycle at this operating condition. In Fig. 12a, the core of the lifted flames is burning at the maximum HAB while the lips attached to the rim of the injectors are burning strongly. The localized flame structures from a single injector downstream of the flame core ($z/D > 2$) encompass a larger non-reacting region. As the cycle begins, the flame in the outer shear layer gradually stretches out from Fig. 12a–c. The core of the flame then propagates upstream rapidly while the post-flame region contracts at higher HAB in Fig. 12d–f. Simultaneously, the flames stabilized in the outer shear layer become weaker. From this maximum upstream location, flame merging appears to occur between the core and outer shear layer locations. This is observed in the left shear layer from Fig. 12f–j as the stronger OH signal moves into the outer region. The flame in the inner shear layer is then lifted further downstream of the injector exit while the flame in the outer shear layer burns more strongly in Fig. 12j–l to close the acoustic cycle.

A similar longitudinal pulsation is seen in the attached flame on the right, albeit it is not as clear since the flame in the inner shear layer

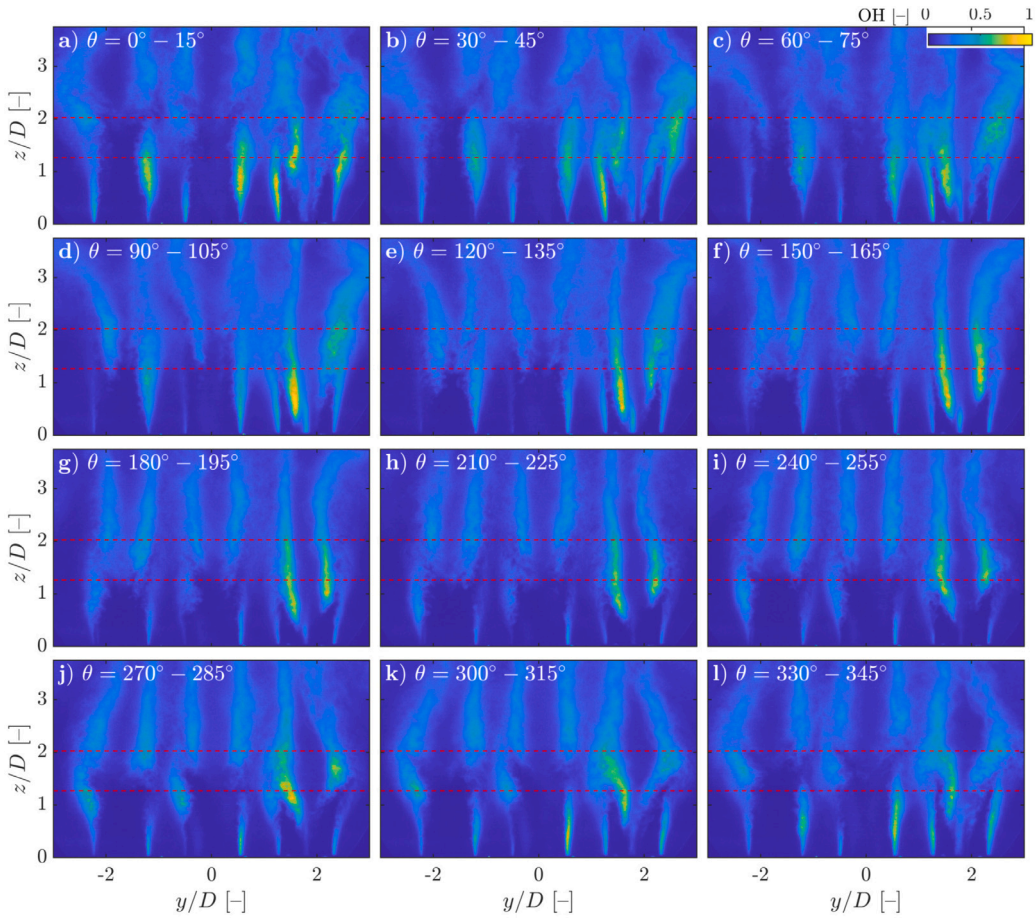

Fig. 12. Phase-averaged mean OH-PLIF fields at the operating condition MFR30 and U_{in} = 50 m/s. Each phase bin covers 15° and only every other bin is shown here for brevity. The red dashed lines indicate the maximum travel of the center of the flame, for the lifted flames, through one cycle.

remains attached to the bluff body of the injector. In addition, there appears to be a spinning motion in the flame as the left and right sides of the flame stabilized in the inner shear layer are moving asynchronously. For these highly 3D flame structures, this could also be caused by the longitudinal mode where the branch on the right side of the frame is better captured at the location where the laser is positioned relative to nozzles and micromix fuel injection. Further investigation with phase-averaged, 3D reconstructed geometries or tomographic measurements would be necessary to fully understand the flame motion.

4. Conclusion

This work presents a first investigation into multi-element premix/micromix injectors for hydrogen combustion performed in the Atmospheric Combustion Rig at the National Research Council Canada. Five additively-manufactured burners enabling an adjustable fuel staging between premixed and micromixed combustion strategies are placed in a cross-shaped array. It provides hot boundary conditions for the central flame and approaches the industrial configuration where these smaller injectors are typically installed in large arrays. This configuration reveals interesting thermoacoustic behavior and exhibits flame–flame interactions in partially-premixed mixtures captured using OH-PLIF to better understand the combustion properties of such complex novel systems.

A significant improvement in flashback limits is observed as the amount of micromixing is increased. The micromix injection prevents traditional flashback into the injector, but can still damage the hardware if the flames are close enough to the exit plane to transfer heat. The flashback velocities are higher for the array than for a single nozzle for all premixing conditions, but a larger increase is observed for predominately premixed mixtures. The hotter boundary conditions, variations in additively-manufactured injectors, and thermoacoustics for multi-element combustion are all partly responsible for the deterioration of the flashback limit in the 5-nozzle array. Significant differences in flashback limits were measured for different array configurations with multiple printed nozzles. While no visible defect could be observed, the flames preferentially attached to specific locations on the injector body before flashback. Such large discrepancies between array configurations highlight the challenges of producing multi-element combustion systems while achieving the same geometry and surface roughness with additive manufacturing. For these multi-element combustion systems, a single injector flashing back for any reason, for example a locally richer mixture, inadequate fuel distribution, or thermoacoustics, could lead to hardware failure for the entire system. A better understanding of the flashback mechanisms within multi-nozzle stratified combustion systems is required to mitigate the risks of engine damage.

The use of micromix injection improved the acoustics of the array compared to predominantly premixed conditions. Reductions in pressure fluctuations by approximately one order of magnitude were observed in the combustor for micromixing fractions greater than 60%. At higher bulk inlet velocities, fewer frequencies are excited and a roughly bimodal spectrum is measured with resonant frequencies of

similar singled-sided amplitudes at ~450, corresponding to an axial full wave through the combustor, and ~2700 Hz. Further modeling of the partially-premixed combustion system will be required to better understand the thermoacoustics of the 5-nozzle array with inhomogeneous heat release rate and non-uniform flame structures. A phase-averaged OH-PLIF sequence at one of the noisiest conditions (U_{in} = 50 m/s and MFR30) captures the limit cycle of the axial full wave at ~450 Hz and shows flame motion of the order of 0.75D for the lifted flames. The pulsating flames show periodically stronger combustion in the outer shear layers than the inner, indicating non-uniform fuel distribution in the stratified mixture.

OH-PLIF images are acquired for various combination of bulk inlet velocity and micromix/premix fuel split (MFR). Instantaneous planar measurements show the wrinkled flame structures obtained for the lean hydrogen conditions studied. The distributed combustion zones are hinted through the analysis of planar images taken through the nozzle centerline axes, but the mean 3D OH reconstruction of a pure micromix flame from 25 different PLIF datasets collected at varying radial locations truly shows the complex flame structures of these micromixed flames. For this injector, distributed, localized flames are spread around the injector in the swirling flow, similar to flower petals around a stem. Even across the 3 injectors studied simultaneously along the laser sheet, open and closed flame petals are observed. Evidence of flame merging are obtained in the 3D reconstruction which might lead to higher pollutant emissions if elongated, hot regions are formed.

The complex three-dimensional, non-axisymmetric flames, and the flame–flame interactions provide many challenges for the application of laser diagnostics to these premix/micromix injectors achieving stratified fuel-air mixtures in a multi-nozzle combustor. This work provides a first investigation of these complex systems and identifies areas for improvement. The dataset collected should help gas turbine manufacturers validate their simulations of partially-premixed combustion to streamline the design process and mitigate the risks and costs of a new injector program.

CRediT authorship contribution statement

Antoine Durocher: Conceptualization, Investigation, Methodology, Writing – original draft, Writing – review & editing, Data curation, Formal analysis. **Luming Fan:** Investigation, Methodology, Writing – review & editing. **Marc Füri:** Conceptualization, Resources, Writing – review & editing, Formal analysis. **Gilles Bourque:** Conceptualization, Resources, Writing – review & editing. **Julien Sirois:** Conceptualization, Resources. **David May:** Conceptualization, Resources. **Jeffrey M. Bergthorson:** Funding acquisition, Supervision, Writing – review & editing. **Sean Yun:** Project administration. **Patrizio Vena:** Conceptualization, Funding acquisition, Supervision, Writing – review & editing.

Declaration of competing interest

The authors declare the following financial interests/personal relationships which may be considered as potential competing interests: Siemens Energy Canada

Data availability

Data will be made available on request.

Acknowledgments

The authors wish to acknowledge the support of the NRC's Low-emission Aviation program (LEAP), the Natural Sciences and Engineering Research Council of Canada (NSERC), Environment and Climate Change Canada (ECCC), and Siemens Energy Canada Limited.

Permission for use

The content of this paper is copyrighted by the National Research Council Canada and Siemens Energy Canada Limited and is licensed for publication and distribution only. Any inquiries regarding permission to use the content of this paper, in whole or in part, for any purpose must be addressed to National Research Council Canada and Siemens Energy Canada Limited directly.

References

[1] Mazloomi K, Gomes C. Hydrogen as an energy carrier: Prospects and challenges. Renew Sustain Energy Rev 2012;16(5):3024–33. http://dx.doi.org/10.1016/j.rser.2012.02.028.

[2] Abe J, Popoola A, Ajenifuja E, Popoola O. Hydrogen energy, economy and storage: Review and recommendation. Int J Hydrogen Energy 2019;44(29):15072–86. http://dx.doi.org/10.1016/j.ijhydene.2019.04.068.

[3] Funke HH-W, Beckmann N, Keinz J, Horikawa A. 30 Years of dry-low-NOx micromix combustor research for hydrogen-rich fuels—An overview of past and present activities. J Eng Gas Turbines Power 2021;143(7). http://dx.doi.org/10.1115/1.4049764.

[4] Noble D, Wu D, Emerson B, Sheppard S, Lieuwen T, Angello L. Assessment of current capabilities and near-term availability of hydrogen-fired gas turbines considering a low-carbon future. J Eng Gas Turbines Power 2021;143(4). http://dx.doi.org/10.1115/1.4049346.

[5] Candel S. Combustion dynamics and control: Progress and challenges. Proc Combust Inst 2002;29(1):1–28. http://dx.doi.org/10.1016/S1540-7489(02)80007-4.

[6] Beita J, Talibi M, Sadasivuni S, Balachandran R. Thermoacoustic instability considerations for high hydrogen combustion in lean premixed gas turbine combustors: A review. Hydrogen 2021;2(1):33–57. http://dx.doi.org/10.3390/hydrogen2010003.

[7] Ciani A, Wood JP, Wickström A, Rørtveit GJ, Steeneveldt R, Pettersen J, et al. Sequential combustion in ansaldo energia gas turbines: The technology enabler for CO2-free, highly efficient power production based on hydrogen. In: Volume 4A: Combustion, fuels, and emissions. American Society of Mechanical Engineers; 2020, http://dx.doi.org/10.1115/GT2020-14794.

[8] Solana-Pérez R, Shcherbanev SA, Dharmaputra B, Ciani A, Noiray N. Combustion regime transition of H_2 flames during steady and transient operation of a sequential combustor. Proc Combust Inst 2022. http://dx.doi.org/10.1016/j.proci.2022.08.014.

[9] Jin U, Kim KT. Experimental investigation of combustion dynamics and NO_x/CO emissions from densely distributed lean-premixed multinozzle $CH_4/C_3H_8/H_2$/air flames. Combust Flame 2021;229:111410. http://dx.doi.org/10.1016/j.combustflame.2021.111410.

[10] Kang H, Kim KT. Combustion dynamics of multi-element lean-premixed hydrogen-air flame ensemble. Combust Flame 2021;233:111585. http://dx.doi.org/10.1016/j.combustflame.2021.111585.

[11] Asai T, Akiyama Y, Dodo S. Development of a state-of-the-art dry low NO_x gas turbine combustor for IGCC with CCS. In: Recent advances in carbon capture and storage. InTech; 2017, http://dx.doi.org/10.5772/66742.

[12] York WD, Ziminsky WS, Yilmaz E. Development and testing of a low NO_x hydrogen combustion system for heavy-duty gas turbines. J Eng Gas Turbines Power 2013;135(2). http://dx.doi.org/10.1115/1.4007733.

[13] Funke HH-W, Beckmann N, Abanteriba S. An overview on dry low NO_x micromix combustor development for hydrogen-rich gas turbine applications. Int J Hydrogen Energy 2019;44(13):6978–90. http://dx.doi.org/10.1016/j.ijhydene.2019.01.161.

[14] Kroniger D, Horikawa A, Funke HH-W, Pfaeffle F, Kishimoto T, Okada K. Experimental and numerical investigation on the effect of pressure on micromix hydrogen combustion. In: Volume 3A: Combustion, fuels, and emissions. American Society of Mechanical Engineers; 2021, http://dx.doi.org/10.1115/GT2021-58926.

[15] Kroniger D, Horikawa A, Okada K, Ashida Y. Novel fuel injector geometry for enhancing the fuel flexibility of a dry low NO_x MicroMix flame. In: Volume 3B: Combustion, fuels, and emissions. American Society of Mechanical Engineers; 2022, http://dx.doi.org/10.1115/GT2022-83025.

[16] Durocher A, Fan L, Francolini B, Furi M, Bourque G, Sirois J, et al. Characterization of a novel am micromix nozzle burning methane to hydrogen. J Eng Gas Turbines Power 2023;1–12. http://dx.doi.org/10.1115/1.4063690.

[17] An Q, Kheirkhah S, Bergthorson J, Yun S, Hwang J, Lee WJ, et al. Flame stabilization mechanisms and shape transitions in a 3D printed, hydrogen enriched, methane/air low-swirl burner. Int J Hydrogen Energy 2021;46(27):14764–79. http://dx.doi.org/10.1016/j.ijhydene.2021.01.112.

[18] Giuliani F, Paulitsch N, Cozzi D, Görtler M, Andracher L. An assessment on the benefits of additive manufacturing regarding new swirler geometries for gas turbine burners. In: Volume 4A: Combustion, fuels, and emissions. American Society of Mechanical Engineers; 2018, http://dx.doi.org/10.1115/GT2018-75165.

[19] Moosbrugger V, Giuliani F, Paulitsch N, Andracher L. Progress in burner design using additive manufacturing with a monolithic approach and added features. In: Volume 4A: Combustion, fuels, and emissions. American Society of Mechanical Engineers; 2019, http://dx.doi.org/10.1115/GT2019-90720.

[20] Rajasegar R, Mitsingas CM, Mayhew EK, Liu Q, Lee T, Yoo J. Development and characterization of additive-manufactured mesoscale combustor array. J Energy Eng 2018;144(3). http://dx.doi.org/10.1061/(ASCE)EY.1943-7897.0000527.

[21] Cho E-S, Jeong H, Hwang J, Kim M. A novel 100% hydrogen gas turbine combustor development for industrial use. In: Volume 3A: Combustion, fuels, and emissions. American Society of Mechanical Engineers; 2022, http://dx.doi.org/10.1115/GT2022-80619.

[22] Bridgeland R, Chapman A, McLellan B, Sofronis P, Fujii Y. Challenges toward achieving a successful hydrogen economy in the US: Potential end-use and infrastructure analysis to the year 2100. Clean Prod Lett 2022;3:100012. http://dx.doi.org/10.1016/j.clpl.2022.100012.

[23] Lee T, Kim KT. Combustion dynamics of lean fully-premixed hydrogen-air flames in a mesoscale multinozzle array. Combust Flame 2020;218:234–46. http://dx.doi.org/10.1016/j.combustflame.2020.04.024.

[24] Fanaca D, Alemela PR, Hirsch C, Sattelmayer T. Comparison of the flow field of a swirl stabilized premixed burner in an annular and a single burner combustion chamber. J Eng Gas Turbines Power 2010;132(7). http://dx.doi.org/10.1115/1.4000120.

[25] Kwong WY, Steinberg AM. Blowoff and reattachment dynamics of a linear multinozzle combustor. J Eng Gas Turbines Power 2019;141(1). http://dx.doi.org/10.1115/1.4041070.

[26] Jella SE, Kwong WY, Steinberg AM, Park JW, Lu T, Bergthorson JM, et al. Attached and lifted flame stabilization in a linear array of swirl injectors. In: Proceedings of the combustion institute, vol. 38, (4):Elsevier Ltd; 2021, p. 6279–87. http://dx.doi.org/10.1016/j.proci.2020.06.009.

[27] Fan L, Savard B, Carlyle S, Nozari M, Naaman R, Fond B, et al. Simultaneous stereo-PIV and OH×CH_2O PLIF measurements in turbulent ultra lean CH_4/H_2 swirling wall-impinging flames. Proc Combust Inst 2022. http://dx.doi.org/10.1016/j.proci.2022.09.039.

[28] Siemens Energy Materials Solutions. Material datasheet nickel alloy inconel 625. Technical report, 2020, URL: https://assets.siemens-energy.com/siemens/assets/api/uuid:c1158c15-a207-4594-9866-91a8a6a04f68/material-datasheet-in625-mp-2020-11-29.pdf.

[29] Schefer R, Kulatilaka W, Patterson B, Settersten T. Visible emission of hydrogen flames. Combust Flame 2009;156(6):1234–41. http://dx.doi.org/10.1016/j.combustflame.2009.01.011.

[30] Li T, Pareja J, Fuest F, Schütte M, Zhou Y, Dreizler A, et al. Tomographic imaging of OH laser-induced fluorescence in laminar and turbulent jet flames. Meas Sci Technol 2018;29(1):015206. http://dx.doi.org/10.1088/1361-6501/aa938a.